

Article

Ion Dynamics at the Carbon Electrode/Electrolyte Interface: Influence of Carbon Nanotubes Types

Freddy Escobar-Teran ^{1,2} , Hubert Perrot ^{1,*}  and Ozlem Sel ¹

¹ Laboratory Interfaces and Electrochemical Systems, LISE, UMR8235, Sorbonne University, CNRS, F-75005 Paris, France; fescobarteran@hotmail.com (F.E.-T.); ozlem.sel@sorbonne-universite.fr (O.S.)

² Department of Exact Sciences, The Armed Forces University-ESPE, Sangolqui 171103, Ecuador

* Correspondence: hubert.perrot@sorbonne-universite.fr

Abstract: Electrochemical quartz crystal microbalance (EQCM) and AC-electrogravimetry methods were employed to study ion dynamics in carbon nanotube base electrodes in NaCl aqueous electrolyte. Two types of carbon nanotubes, Double Wall Carbon Nanotube (DWCNT) and Multi Wall Carbon Nanotube (MWCNT), were chosen due to their variable morphology of pores and structure properties. The effect of pore morphology/structure on the capacitive charge storage mechanisms demonstrated that DWCNT base electrodes are the best candidates for energy storage applications in terms of current variation and specific surface area. Furthermore, the mass change obtained via EQCM showed that DWCNT films is 1.5 times greater than MWCNT films in the same potential range. In this way, the permselectivity of DWCNT films showed cation exchange preference at cathode potentials while MWCNT films showed anion exchange preference at anode potentials. The relative concentration obtained from AC-electrogravimetry confirm that DWCNT base electrodes are the best candidates for charge storage capacity electrodes, since they can accommodate higher concentration of charged species than MWCNT base electrodes.

Keywords: carbon nanotubes; DWCNT; MWCNT; electrochemical quartz crystal microbalance; EQCM; electrode/electrolyte interface; ion transfer



Citation: Escobar-Teran, F.; Perrot, H.; Sel, O. Ion Dynamics at the Carbon Electrode/Electrolyte Interface: Influence of Carbon Nanotubes Types. *Materials* **2022**, *15*, 1867. <https://doi.org/10.3390/ma15051867>

Academic Editor: Kamila Sadowska

Received: 10 December 2021

Accepted: 14 February 2022

Published: 2 March 2022

Publisher's Note: MDPI stays neutral with regard to jurisdictional claims in published maps and institutional affiliations.



Copyright: © 2022 by the authors. Licensee MDPI, Basel, Switzerland. This article is an open access article distributed under the terms and conditions of the Creative Commons Attribution (CC BY) license (<https://creativecommons.org/licenses/by/4.0/>).

1. Introduction

The development of energy storage systems (supercapacitors/batteries) to decrease the energy consumption coming from fossil fuels is a way towards a more environmentally friendly society. However, the efficiency of these electrochemical devices depends on the elements constituting them such as the electrode material, which plays an important role to achieve better supercapacitor performances [1,2].

In supercapacitors, the charge storage is based on a reversible adsorption of electrolyte ions towards the surface of electrodes [3–8]. Therefore, the selection of the electrode materials is important due to a certain number of parameters such as: specific surface area, porosity, structure, electrical conductivity, surface wettability, and electrochemical stability to improve the performance of electrodes [2,9–12]. In this way, carbon nanotubes have been used for supercapacitors due to their novel properties such as high electrical conductivity, high charge transport capability, unique pore structure and high specific surface area where the charges are continuously distributed [13,14].

However, the ion dynamics studies at the interfaces are experimentally difficult because there are not many appropriate electrochemical or physico-chemical methods that provide direct access to this kind of information.

Electrochemical quartz crystal microbalance (EQCM) has been extensively used to investigate the charge storage mechanisms in porous materials. EQCM is a powerful in situ technique to measure ionic fluxes at the electrode interfaces, for which current responses (ΔI) and global gravimetric changes (Δm) at the electrode/electrolyte interface are monitored

during the electrochemical process. Over the past decade, Levi et al. [15–20] have widely employed EQCM to study the charge–compensation mechanism in carbon micropores and, particularly, the effect of specific adsorption of ions with different sizes. Continuing these achievements, EQCM was also used to investigate the charge compensation mechanism between electrode/electrolyte interface [21] and the hydration/solvation effect on the capacitive performance [22,23]. Recently, EQCM has been employed to study the electrolyte concentration effect on the capacitive behavior as well as the compositional changes in porous films [24]. Finally, EQCM combined with nuclear magnetic resonance (NMR) has been employed to understand in a deep manner the charge mechanism in the electrical double layer [25].

Another interesting aspect of the EQCM is the capability to estimate mass and charge variations simultaneously, which provides access to the derivation of the global mass per mole of electrons (MPE) exchanged at the electrochemical interface. In this way, the MPE corresponds to its molar mass when one species is exchanged, but, if multiple ion transfer occurs, EQCM remains limited in interpreting the contribution of different species [22,24]. In order to identify the contribution of different species, EQCM equations were developed incorporating Donnan type electrical double layer models [26]. Furthermore, EQCM with dissipation monitoring (EQCM-D) can be used to study the viscoelastic properties e.g., formation of a solid electrolyte interface (SEI) layer as well as the complex mass changes of the electrodes [27–30]. This acoustic technique permits to identify the effect of several parameters such as the nature of the electrolytes/ions or the binder on the structure change of the electrodes [31].

Here, an alternative electrochemical and gravimetric method called AC-electrogravimetry was used to complement the EQCM based methods in the energy storage domain. AC-electrogravimetric methodology has been used to study the charge compensation mechanisms in carbon nanotubes [32,33], reduced graphene oxide [34,35], pseudocapacitive metal oxide-based electrodes [25,36] and nanocomposite electrodes [34,37]. Recently, it has been employed to investigate the ion insertion mechanisms in aqueous proton-based batteries [38]. AC-electrogravimetry is a multi-scale coupled electrogravimetric method (quartz crystal microbalance and electrochemical impedance) through which it provides relevant information concerning: (i) identification and kinetic of electroadsorption/desorption of species at the electrode/electrolyte interface, (ii) separation of the charged and non-charged species involved at the electrode/electrolyte interface, and (iii) the relative concentration variations of the species within the material. Therefore, the AC-electrogravimetric methodology was proposed here to study/compare the capacitive behavior in different types of carbon nanotube electrodes.

2. Materials and Methods

2.1. Materials

Double Wall CNT (755141-1G, length: 3 μm and diameter: 3.5 nm) and Multi Wall CNT (75517-1G, length: 1 μm and diameter: 9.5) were acquired at the Sigma Aldrich Company (St. Louis, MO, USA).

2.2. CNT Thin Films' Electrode Preparation

CNT films were prepared according to the method described in previous papers [32,34,39]. A solution containing 90% carbon (9 mg) CNT powder and 10% (1 mg) poly(vinylidene fluoride-hexafluoropropylene) (PVDF-HFP) polymer binder in 10 mL of N-methyl-2-pyrrolidone was prepared to elaborate CNT films. Around 8 μL of this solution were deposited through the “drop-casting” method on a gold electrode, which has an effective surface area of 0.20 cm^2 and remains connected to a quartz crystal resonator (9 MHz-AWS, Valencia, Spain). After that, the carbon films followed a heat treatment with a heating rating of $\sim 5\text{ }^\circ\text{C min}^{-1}$ until 120 $^\circ\text{C}$ for 30 min. This treatment was necessary to eliminate the residual solvent and improve the linkage of films on the QCM electrode. The deposited mass was calculated by using the Sauerbrey equation, $\Delta f_m = -k_s \Delta m$, where Δf_m is the microbal-

ance frequency change, k_s is the experimental calibration constant ($16.3 \times 10^{+7} \text{ Hz/g}\cdot\text{cm}^{-2}$) and Δm corresponds to the mass change. It was obtained by measuring Δf_m , microbalance frequency change before and after deposition.

2.3. Morphological and Physical Characterizations

The CNT powders were characterized by Brunauer–Emmett–Teller methods (BET, Passy, France), X-ray diffraction (XRD, Malvern, United Kingdom) and high-resolution transmission electron microscopy (HR-TEM, Croissy sur Seine, France). Details about the characteristics and selected parameters of these equipment are described in a previous paper [33].

Field emission gun scanning electron microscopy (FEG-SEM, Zeiss, Ultra 55, Jena, Germany) was also employed to investigate the surface morphology of the CNT films. In our experiments, FEG-SEM (Field Emission Gun-Scanning Electron Microscope) provides a very highest resolution imaging compared to regular SEM. The samples were previously prepared on an aluminum stub with a conductive carbon tape and sputter-coated with gold (JEOL JFC-1300 Auto fine coater, Croissy sur Seine, France).

2.4. EQCM and AC-Electrogravimetric Characterization

EQCM measurements were carried out in NaCl aqueous solutions and using a three-electrode configuration. A lab-made QCM device (Miller oscillator, Paris, France) was employed to measure frequency shift (Δf) of the quartz crystal resonators. A gold electrode of the quartz resonator was used as the working electrode. Platinum grid and Ag/AgCl (3 M KCl) were used as a counter and reference electrode, respectively (See Figure 1). The gravimetric regime was assured by keeping the film thickness acoustically thin (<200 nm).

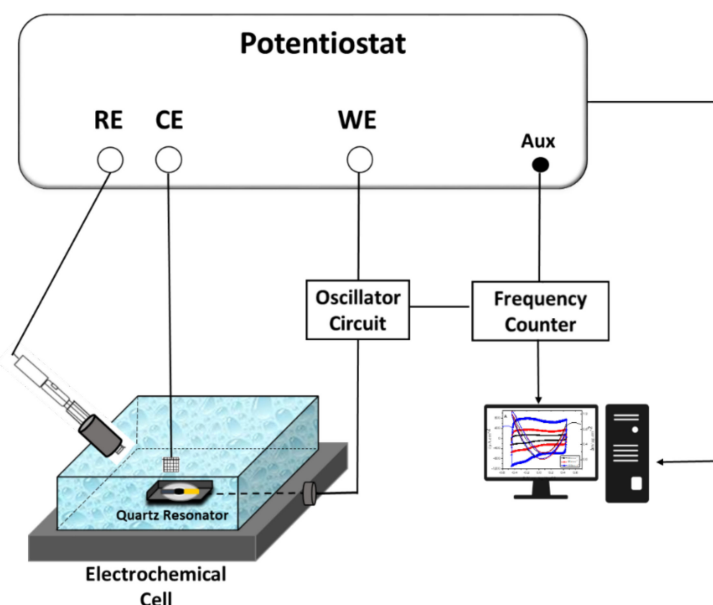


Figure 1. Experimental set-up of an EQCM.

A QCM set-up connected to a four-channel frequency response analyzer (FRA, Solartron 1254, Élan-court, France) and a lab-made potentiostat (SOLETEM-PGSTAT, Paris, France) were employed to obtain AC-electrogravimetric measurements. The QCM measurements were carried out under dynamic regime, following the potential modulation operating at various frequencies, the electrochemical system being polarized at selected potentials.

In order to obtain a dynamic regime, a sinusoidal small amplitude potential perturbation was superimposed. The frequency intervals were from 63 KHz to 10 mHz. The AC response, ΔI , of the electrochemical system and the mass change, Δm , of the working electrode were simultaneously measured, which resulted in the electrogravimetric

TF, $(\Delta m/\Delta E(\omega))$ and the electrical TF $(\Delta E/\Delta I(\omega))$. These transfer functions were obtained simultaneously at a given potential and frequency modulation, f (pulsation, $\omega = 2\pi f$). The working principle and AC-electrogravimetric measurement setup have been detailed previously [34,36,40,41].

3. Results and Discussion

3.1. Material Characteristics

DWCNTs and MWCNTs constituting the composite electrodes were characterized by HRTEM. The images in Figure 2A,C indicate that the diameters of the DWCNTs and MWCNTs are about ~4 nm and ~8 nm, respectively. Thus, it indicates a large difference between the two samples at this level. Nitrogen sorption measurements and XRD were used to characterize the specific surface area and crystallinity of the CNTs. The Brunauer–Emmett–Teller (BET) specific surface area of the DWCNTs and MWCNTs was estimated to be $552 \text{ m}^2 \cdot \text{g}^{-1}$ and $300 \text{ m}^2 \cdot \text{g}^{-1}$, respectively, and the crystallinity attributed to the hexagonal graphitic structure [42] was observed on (002) and (001) reflections (see Figures S1 and S2). BET demonstrates clearly a significant difference between the two materials: DWCNT films give a pore size around 3–4 nm while MWCNTs films show two pore sizes, a first one around 3–4 nm and a second one around 25 nm. On the contrary, the two XRD spectra give similar results, which indicates a similar crystallinity. To assume an equivalent hydrophobic character, successive electrochemical cycles were performed. By this way, an equivalent and optimized electrolyte accessibility is obtained. Then, the CNT electrodes were deposited on the gold patterned quartz resonators. For that, the PVDF-HFP was used as a binder polymer to adhere to the CNT on the gold quartz resonator. Figure 2B,D show an FEG-SEM image of the DWCNT and MWCNT film electrodes, which reveal a high-density of CNT bundles. The surface roughness was not directly estimated, but FEG-SEM images do not show a strong difference about this point between the two films.

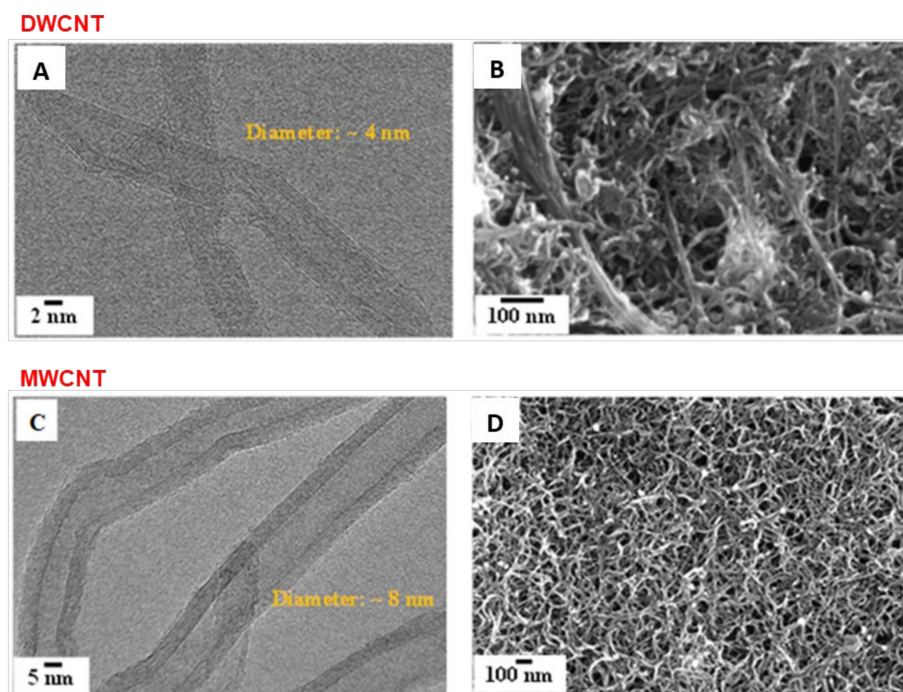


Figure 2. HRTEM images of the DWCNTs (A) MWCNTs (C) and FEG-SEM images of DWCNT (B), MWCNT (D) based thin films deposited on the gold patterned quartz resonator.

3.2. EQCM Study of CNTs in 0.5 M NaCl

The EQCM results of CNT thin films obtained in aqueous electrolytes of 0.5 M NaCl are shown in Figure 3A, and a growing capacitive current is observed when the scan

rate increases (Figure 3A,B) for all the films. In addition, DWCNT films show a higher capacitive current than MWCNT films and even more than SWCNT described in the previous paper [32]. This difference in current is probably due to the pore structure of the materials and its accessibility to the electrolyte ions, which is contradictory with the specific surface area determined on the CNT powder but not with the CNT films. In this study, DWCNT and MWCNT films show quasi-rectangular shaped responses indicating that the charge storage capacity is mainly due to the reversible adsorption/desorption of electrolyte ions. The slight distortion from a perfect rectangular shape is attributed to the presence of a slight faradaic contribution to the charge storage as already mentioned [32,33].

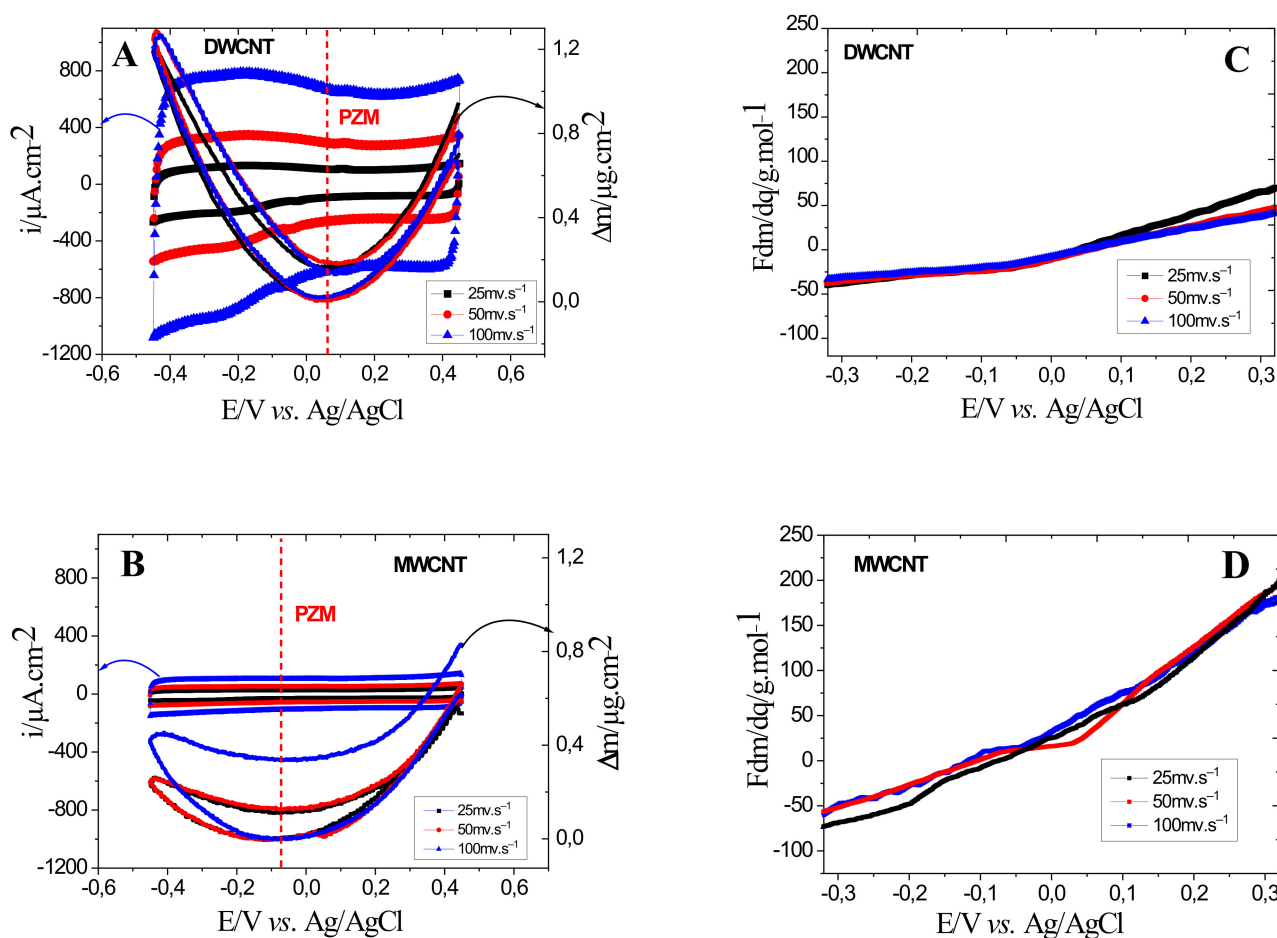


Figure 3. EQCM results of DWCNT (A), and MWCNT (B) measured in a 0.5 M NaCl aqueous electrolyte. The average molecular weight values of the species involved in the electrochemical process showed as a function of the potential obtained from the reduction branch of EQCM data are presented in (C,D).

Regarding the mass changes, the DWCNT and MWCNT follow the same order as the current values, i.e., $\Delta m_{DWCNT} > \Delta m_{MWCNT}$. In addition, the reversibility of the mass response is better appreciated in DWCNT than in MWCNT (Figure 3A,B), where a large hysteresis was observed in MWCNT. For the DWCNT, the mass change is higher at cathodic potentials than at anodic potentials, while, in MWCNT, the mass change is slightly more significant at anodic potentials than at cathodic potentials. It is also observed that the PZC is shifted slightly towards more cathodic potentials (Figure 3B). The PZC or PZM is the point where the charge/mass is equal to zero, and this corresponds to the potential of 0.075 ± 0.25 V for DWCNT and -0.075 ± 0.25 V for MWCNT follows the following order: $PZM_{DWCNT} < PZM_{MWCNT}$. In other words, DWCNT films show cations exchange preference, while MWCNT films show anions exchange preference in the same potential

range. In addition, the V-shape observed in the mass changes (Figure 3A,B) is due to the selective adsorption/desorption of cationic and anionic species in the potential range [32,42].

The average molecular weight values, $\frac{Fdm}{dq}$ ($= F \frac{dm}{dq} x \frac{1}{i}$), of the species involved in the electrochemical process showed as a function of the potential are obtained from the reduction branch of EQCM data presented in Figure 3A,B.

Figure 3C,D show the average molecular weight values of the electroadsorbed species if only one ion is transferred. The values are calculated as a function of the applied potential in the NaCl electrolyte. The values vary in the range of 50 to $-35 \text{ g}\cdot\text{mol}^{-1}$ and 180 to $-70 \text{ g}\cdot\text{mol}^{-1}$, for the DWCNT and MWCNT thin films, respectively. From the two Figure 3C,D, it should be noted that, for anodic potentials, positive Fdm/dq values are estimated, which corresponds to anion contribution. As for cathodic potentials, negative Fdm/dq values were calculated indicating the cation contribution. In all the cases, higher or lower atomic weight compared to Na^+ or Cl^- ions are found, which indicates a complex ion transfer behavior associated with solvent contribution. The observed higher values further indicate that the ions are hydrated and/or accompanied by free solvent molecules during their transfer in the same direction. Particularly in MWCNT, higher values at anodic potentials are observed, which could correspond to anions accompanied by free solvent molecules.

3.3. AC-Electrogravimetric Study of CNT Thin Film Electrodes in 0.5 M NaCl

Analysis of AC-electrogravimetric responses of DWCNT and MWCNT film electrodes are presented in Figure 4 in a comparative manner at a selected potential (-0.4 V) in the cathodic part.

Table 1. K_i (kinetics of transfer), and G_i (inverse of the transfer resistance), Rt_i (transfer resistance) values extracted from the fitting results from AC-electrogravimetric measurements in aqueous 0.5 M NaCl at -0.4 V vs. Ag/AgCl for DWCNT and MWCNT films.

CNT Types/ Species	M_i ($\text{g}\cdot\text{mol}^{-1}$)	Species Identification	K_i ($\text{cm}\cdot\text{s}^{-1}$)	G_i ($\text{mol}\cdot\text{s}^{-1}\cdot\text{cm}^{-2}\cdot\text{V}^{-1}$)	$Rt_i = 1/FG_i$ $\text{ohm}\cdot\text{cm}^2$
DWCNT					
c2	23 + 18	$\text{Na}^+\cdot\text{H}_2\text{O}$	2.89×10^{-3}	4.65×10^{-6}	2.22
s	18	H_2O	6.28×10^{-4}	9.11×10^{-7}	11.37
c1	1	H^+	3.64×10^{-5}	1.39×10^{-8}	745.52
MWCNT					
c2	23 + 18	$\text{Na}^+\cdot\text{H}_2\text{O}$	5.66×10^{-3}	1.10×10^{-6}	9.42
s	18	H_2O	5.03×10^{-4}	5.23×10^{-6}	1.98
c1	1	H^+	2.39×10^{-4}	3.58×10^{-9}	2894.61

First, the charge/potential transfer functions (TFs), $\frac{\Delta q}{\Delta E}(\omega)$, permit a suitable separation of the ionic contributions, however, without any possibility to identify the ionic species involved.

In Figure 4A and C for DWCNT and MWCNT films, respectively, one big loop is observed, which can be assigned to only one species. However, two species can also be assigned regarding the fact that the time constants of ions are not really different from each other.

To clarify these ideas, the mass /potential transfer functions, $\frac{\Delta m}{\Delta E}(\omega)$, is used. Figure 4B,D show a big loop in the third quadrant from 100 to 1 Hz, which is characteristic of cation and free solvent molecules in the same flux directions, as described previously [40,41].

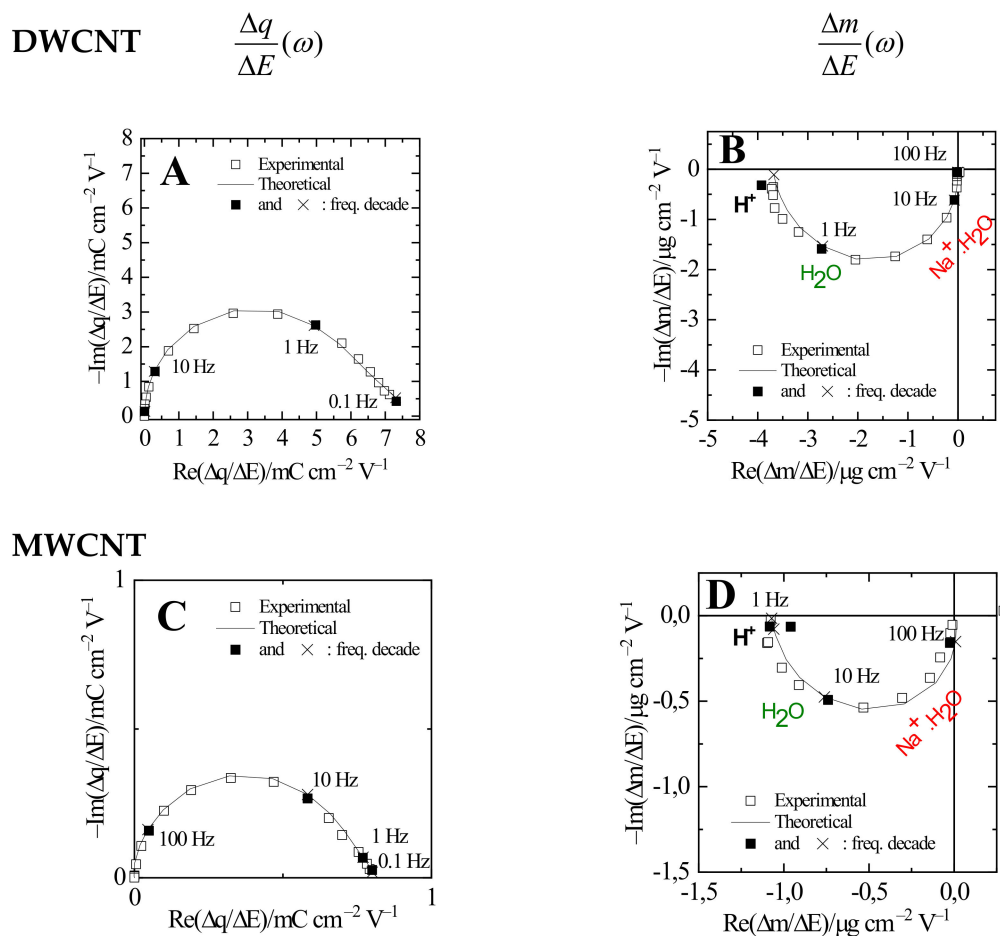


Figure 4. Experimental and theoretical AC-electrogravimetric data of the CNT thin films in 0.5 M NaCl measured at -0.4 V vs. Ag/AgCl. (A,C) $\frac{\Delta q}{\Delta E}(\omega)$, (B,D) $\frac{\Delta m}{\Delta E}(\omega)$. The parameter values of K_i , G_i and Rt_i are shown in Table 1.

The experimental TFs in Figure 4 were fitted using Equations (A2) and (A3) (Appendix A): firstly, the number of species intervening and their respective K_i and G_i parameters were estimated from $\frac{\Delta E}{\Delta I}(\omega)$ or $\frac{\Delta q}{\Delta E}(\omega)$. These two key parameters were also used for the fitting of the experimental $\frac{\Delta m}{\Delta E}(\omega)$ TF. Then, identification of the involved species was achieved by fitting the experimental data with the theoretical $\frac{\Delta m}{\Delta E}(\omega)$ TF, which is shown in Equation (A4) where the molar masses of the species (M_i) intervene in this equation. Here, for two films, the molar masse represents H^+ (c1) and $Na^+ \cdot H_2O$ (c2) for cations and free solvent (s) molecules in the same flux direction (Figure 4). Furthermore, at selected potential (-0.4 V), there are no anion contributions, which is coherent in this potential region [32,33]. In our experiments, the transport inside the pores is not clearly seen as shown in the EIS responses (Figures S3C and S4C); the typical characteristic slope around 45° slope is not observed here. For this reason, our model does not take into account this effect here.

The presence of two different cationic species and the free solvent molecules contribution estimated by simulating the experimental data was further confirmed by a fair analysis of the partial electrogravimetric transfer functions, for example, by removing the c2 contribution and calculating $\left. \frac{\Delta q}{\Delta E} \right|_{th}^{c1s}(\omega)$, by removing the c1 contribution and calculating $\left. \frac{\Delta q}{\Delta E} \right|_{th}^{c2s}(\omega)$, (Equations (A5) and (A6), no anion contribution at -0.4 V). The fitting results concerning the partial electrogravimetric transfer functions are given in Figures S3 and S4A,B. A good fit also appears for the partial TFs including the same group of parameters, reinforcing the hypothesis of the different ion contributions (Table 1).

In addition, the species contribution was seen previously using electrochemical modulation showing different kinetics of transfer [43] e.g., Hillman et al. monitored the kinetic of species in nickel hydroxide thin films by combining EQCM and probe beam deflection (PBD) [44–46].

Figure 4 shows the AC-electrogravimetric results at -0.4 V vs. Ag/AgCl. In fact, it was measured from -0.45 V to 0.45 V vs. Ag/AgCl to have a complete electrochemical exploration of our system. The nature of the species (M_i) and the corresponding K_i and G_i constants were estimated as a function of potential [34,36,47].

Figure 5 shows the variation of the constant transfer kinetics, K_i , of the species as a function of the applied potential. Based on the K_i values presented in Figure 5A,B, the $\text{Na}^+\cdot\text{H}_2\text{O}$ and Cl^- ions are the fastest of all species for SWCNT and MWCNT films. Here, the number of water molecules associated with the sodium ions is found to be $n = 1$ for all the potentials. Furthermore, the transfer kinetics of free water molecules are somewhat close to the values of the chlorine ions at anode potentials. In addition, these water molecules accompany the transfer of $\text{Na}^+\cdot\text{H}_2\text{O}$ and Cl^- , most likely due to an electrodragging phenomena [32,33].

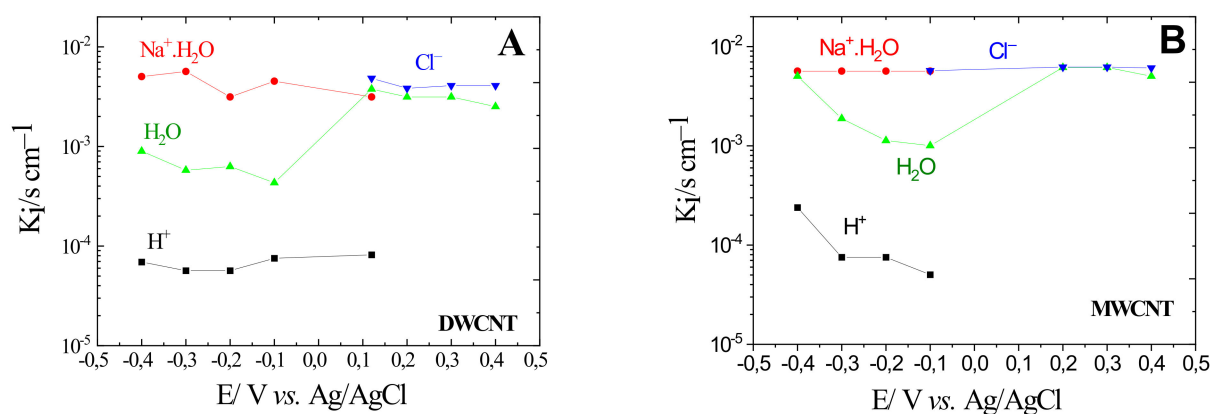


Figure 5. Kinetic constants of interfacial transfer, K_i , DWCNT (A), MWCNT (B) estimated from the fitting of the AC-electrogravimetric data and measured in aqueous 0.5M NaCl.

Finally, the H^+ ion is the slowest species at cathodic potentials for DWCNT and MWCNT films (Figure 5A,B) showing a similar order of magnitude of K_i values, which is coherent with their substantially lower concentration in the media.

In order to quantify the role of each species, $\frac{\Delta C_i}{\Delta E} \Big|_{\omega \rightarrow 0} = -\frac{G_i}{K_i}$ has been calculated as a function of the applied potential using the parameters given by the AC-electrogravimetric fitting. Figure 6 shows the integration of $\frac{\Delta C_i}{\Delta E} \Big|_{\omega \rightarrow 0}$ against potential gives the relative concentration change, $(C_i - C_0)$ of the charged and non-charged species. For MWCNTs (Figure 6B), the $(C_i - C_0)$ values of the H_2O are higher than the $(C_i - C_0)$ values of the $\text{Na}^+\cdot\text{H}_2\text{O}$, Cl^- and H^+ .

In contrast to MWCNT, in DWCNTs, the evolution of relative concentration of species presents a different trend. In comparison with the other species, the $(C_i - C_0)$ values of the $\text{Na}^+\cdot\text{H}_2\text{O}$ are higher than the $(C_i - C_0)$ values of H^+ and H_2O at cathode potentials (Figure 6A). In conclusion, these results indicate that DWCNTs appear to be the best candidate for charge storage capacity electrodes, since it can accommodate a higher concentration of charged species in DWCNTs than in MWCNTs. This result can be attributed to the difference of material form illustrated by the difference of specific surface, which is higher in the case of the DWCNTs, almost two times higher, compared with the value of the MWCNTs. A higher capacitance was also found, in comparison with values given by compact films, with different nanostructured materials as titanium dioxide based composite nanotube-arrays, MnO_2 electrodes, or activated carbon nanoparticles [48–50].

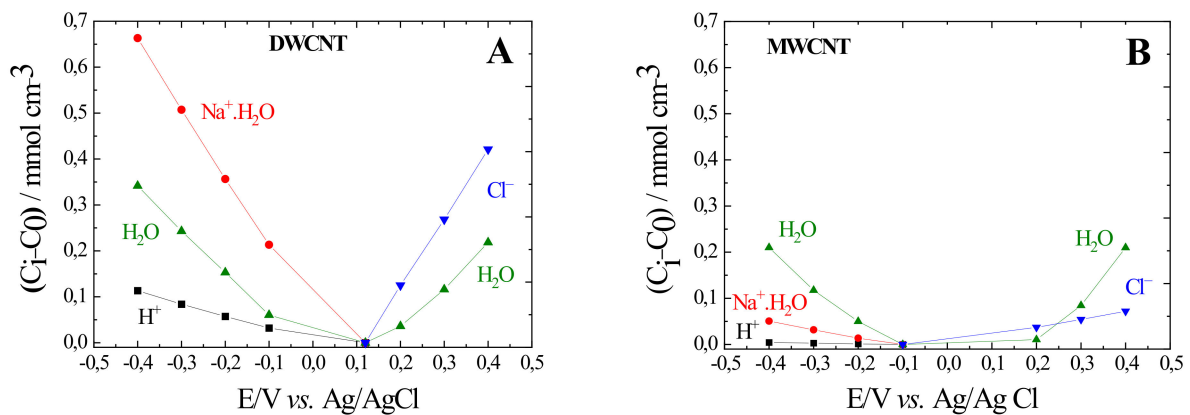


Figure 6. Evolution of the relative concentration, $C_i - C_0$, for DWCNT (A), MWCNT (B) of the charged and non-charged species over the applied potential and measured in aqueous 0.5M NaCl.

4. Conclusions

Carbon nanotubes (CNTs) of “double-walled” (DWCNT), and “multi-walled” (MWCNT) films were elaborated on gold electrodes of microbalance and tested in NaCl aqueous electrolyte. The effect of pore morphology/structure but also roughness or hydrophilicity over the classical electrochemical responses demonstrated that DWCNT are better candidates for energy storage applications than MWCNT base electrodes in terms of current/mass variation and permselectivity of cations. The mass change obtained via EQCM showed that DWCNT films are 1.5 times bigger than MWCNT films in the same range of potential. In this way, the permselectivity of DWCNT films showed cation exchange preference for cathode potentials while MWCNT films showed anion exchange preference for anode potentials. The relative concentration obtained from AC-electrogravimetry confirms that DWCNT base electrodes are the best candidates for polarizable electrodes, since they can accommodate a higher concentration of charged species than MWCNT and even more than SWCNT base electrodes described in the previous paper [32].

Supplementary Materials: The following supporting information can be downloaded at: <https://www.mdpi.com/article/10.3390/ma15051867/s1>. Figures S1 and S2 XRD Spectra, Nitrogen sorption isotherm and the pore size distribution (PSD). Figures S3 and S4 experimental and theoretical AC-electrogravimetric data of the CNT thin films.

Author Contributions: F.E.-T. performed the experiments; H.P. and O.S. planned the experiments; F.E.-T., H.P. and O.S. analyzed the data; H.P. and O.S. contributed to the original draft preparation and revision; O.S. wrote, revised and edited the paper with discussions mainly with H.P. All authors have read and agreed to the published version of the manuscript.

Funding: F.E.-T. thanks the (Secrétariat National pour l’Enseignement Supérieur, la Science, la Technologie et l’Innovation (SENESCYT)-Ecuator for the financial support during his Ph.D. thesis.

Conflicts of Interest: The authors declare no conflict of interest.

Appendix A

For different types of CNT films, the concentration transfer function, $\frac{\Delta C_i}{\Delta E} \Big|_{th}(\omega)$, of cation1 (c_1), cation 2 (c_2), anion (a), and free solvent (s) were calculated through:

$$\frac{\Delta C_i}{\Delta E} \Big|_{th}(\omega) = \frac{-G_i}{j\omega d_f + K_i} \quad (A1)$$

where $\omega = 2\pi f$ is the pulsation, d_f is the film thickness, K_i represents the kinetics transfer, whereas G_i describes the ease/difficulty of ionic species (c_1 and c_2) to be transferred at the

electrode/electrolyte interface. In addition, the transfer resistance, Rt_i , can be determined through G_i using the following expression: $Rt_i = 1/FG_i$, where F is the Faraday number [38–40].

The experimental data of the electrochemical impedance $\left. \frac{\Delta E}{\Delta I} \right|_{th}(\omega)$ and the charge/potential TF, $\left. \frac{\Delta q}{\Delta E} \right|_{th}(\omega)$, were fitted using theoretical transfer functions given in Equations (A2) and (A3). In this case, two cations, $c1$ and $c2$ and anion, a , are involved in the charge compensation process:

$$\left. \frac{\Delta E}{\Delta I} \right|_{th}(\omega) = \left[j\omega d_f \left(\frac{G_{c1}}{j\omega d_f + K_{c1}} + \frac{G_{c2}}{j\omega d_f + K_{c2}} - \frac{G_a}{j\omega d_f + K_a} \right) \right]^{-1} \quad (A2)$$

$$\left. \frac{\Delta q}{\Delta E} \right|_{th}(\omega) = d_f F \left(\frac{G_{c1}}{j\omega d_f + K_{c1}} + \frac{G_{c2}}{j\omega d_f + K_{c2}} - \frac{G_a}{j\omega d_f + K_a} \right) \quad (A3)$$

The theoretical electrogravimetric transfer function, $\left. \frac{\Delta m}{\Delta E} \right|_{th}(\omega)$, can be estimated, taking into account the charged/uncharged species contribution:

$$\left. \frac{\Delta m}{\Delta E} \right|_{th}(\omega) = d_f \left(M_{c1} \frac{G_{c1}}{j\omega d_f + K_{c1}} + M_{c2} \frac{G_{c2}}{j\omega d_f + K_{c2}} + M_a \frac{G_a}{j\omega d_f + K_a} + M_s \frac{G_s}{j\omega d_f + K_s} \right) \quad (A4)$$

In Equation (A4), M_{c1} , M_{c2} , M_a and M_s are the atomic weight of involved species.

From the theoretical overall electrogravimetric transfer function (Equation (A4)), it is possible to calculate the theoretical partial transfer functions by removing the $c2$ contribution, calculating $\left. \frac{\Delta m}{\Delta E} \right|_{th}^{c1as}(\omega)$; or the $c1$ contribution, calculating; $\left. \frac{\Delta m}{\Delta E} \right|_{th}^{c2as}(\omega)$; or the anion contribution calculating; $\left. \frac{\Delta m}{\Delta E} \right|_{th}^{c1c2s}(\omega)$, as shown in the following equations:

$$\left. \frac{\Delta m}{\Delta E} \right|_{th}^{c1as}(\omega) = d_f \left((M_{c1} - M_{c2}) \frac{G_{c1}}{j\omega d_f + K_{c1}} + (M_a - M_{c2}) \frac{G_a}{j\omega d_f + K_a} + M_s \frac{G_s}{j\omega d_f + K_s} \right) \quad (A5)$$

$$\left. \frac{\Delta m}{\Delta E} \right|_{th}^{c2as}(\omega) = d_f \left((M_{c2} - M_{c1}) \frac{G_{c2}}{j\omega d_f + K_{c2}} + (M_a - M_{c1}) \frac{G_a}{j\omega d_f + K_a} + M_s \frac{G_s}{j\omega d_f + K_s} \right) \quad (A6)$$

$$\left. \frac{\Delta m}{\Delta E} \right|_{th}^{c1c2s}(\omega) = d_f \left((M_{c1} - M_{c2}) \frac{G_{c1}}{j\omega d_f + K_{c1}} + (M_{c2} - M_{c1}) \frac{G_{c2}}{j\omega d_f + K_{c2}} + M_s \frac{G_s}{j\omega d_f + K_s} \right) \quad (A7)$$

These last estimated partial transfer functions correspond to a key point of our AC-electrogravimetric technique. Indeed, this cross-checking allows a fair validation of our measurements to be performed.

References

- Béguin, F.; Presser, V.; Balducci, A.; Frackowiak, E. Carbons and Electrolytes for Advanced Supercapacitors. *Adv. Mater.* **2014**, *26*, 2219–2251. [CrossRef] [PubMed]
- Béguin, F.; Raymundo-Piñero, E. Nanocarbons for Supercapacitors. In *Batteries for Sustainability*; Meyers, R., Ed.; Springer: Berlin/Heidelberg, Germany, 2013; pp. 393–421.
- Ganfoud, N.; Sene, A.; Haefele, M.; Marin-Lafèche, A.; Daffos, B.; Taberna, P.-L.; Salanne, M.; Simon, P.; Rotenberg, B. Effect of the carbon microporous structure on the capacitance of aqueous supercapacitors. *Energy Storage Mater.* **2019**, *21*, 190–195. [CrossRef]
- Pandolfo, A.; Hollenkamp, A. Carbon properties and their role in supercapacitors. *J. Power Sources* **2006**, *157*, 11–27. [CrossRef]
- Wu, Y.; Ye, J.; Jiang, G.; Ni, K.; Shu, N.; Taberna, P.; Zhu, Y.; Simon, P. Electrochemical Characterization of Single Layer Graphene/Electrolyte Interface: Effect of Solvent on the Interfacial Capacitance. *Angew. Chem. Int. Ed.* **2021**, *60*, 13317–13322. [CrossRef]
- Bouzina, A.; Perrot, H.; Sel, O.; Debiemme-Chouvy, C. Preventing Graphene from Restacking via Bioinspired Chemical Inserts: Toward a Superior 2D Micro-supercapacitor Electrode. *ACS Appl. Nano Mater.* **2021**, *4*, 4964–4973. [CrossRef]
- Down, M.P.; Banks, C.E. 2D materials as the basis of supercapacitor devices. In *2D Nanomaterials for Energy Applications*; Elsevier: Amsterdam, The Netherlands, 2020; pp. 97–130. [CrossRef]

8. Islam, M.; Alam, M.T.; Okajima, T.; Ohsaka, T. Electrical Double Layer Structure in Ionic Liquids: An Understanding of the Unusual Capacitance–Potential Curve at a Nonmetallic Electrode. *J. Phys. Chem. C* **2009**, *113*, 3386–3389. [[CrossRef](#)]
9. Simon, P.; Gogotsi, Y. Materials for electrochemical capacitors. *Nanosci. Technol.* **2009**, *7*, 320–329. [[CrossRef](#)]
10. Pan, H.; Li, J.; Feng, Y.P. Carbon Nanotubes for Supercapacitor. *Nanoscale Res. Lett.* **2010**, *5*, 654–668. [[CrossRef](#)]
11. Ratajczak, P.; Suss, M.; Kaasik, F.; Béguin, F. Carbon electrodes for capacitive technologies. *Energy Storage Mater.* **2019**, *16*, 126–145. [[CrossRef](#)]
12. Shao, H.; Wu, Y.-C.; Lin, Z.; Taberna, P.-L.; Simon, P. Nanoporous carbon for electrochemical capacitive energy storage. *Chem. Soc. Rev.* **2020**, *49*, 3005–3039. [[CrossRef](#)] [[PubMed](#)]
13. Yang, Z.; Tian, J.; Yin, Z.; Cui, C.; Qian, W.; Wei, F. Carbon nanotube- and graphene-based nanomaterials and applications in high-voltage supercapacitor: A review. *Carbon* **2019**, *141*, 467–480. [[CrossRef](#)]
14. Simon, P.; Gogotsi, Y. Capacitive Energy Storage in Nanostructured Carbon–Electrolyte Systems. *Accounts Chem. Res.* **2013**, *46*, 1094–1103. [[CrossRef](#)] [[PubMed](#)]
15. Levi, M.D.; Levy, N.; Sigalov, S.; Salitra, G.; Aurbach, D.; Maier, J. Electrochemical Quartz Crystal Microbalance (EQCM) Studies of Ions and Solvents Insertion into Highly Porous Activated Carbons. *J. Am. Chem. Soc.* **2010**, *132*, 13220–13222. [[CrossRef](#)]
16. Levi, M.D.; Salitra, G.; Levy, N.; Aurbach, D.; Maier, J. Application of a quartz-crystal microbalance to measure ionic fluxes in microporous carbons for energy storage. *Nat. Mater.* **2009**, *8*, 872–875. [[CrossRef](#)]
17. Levi, M.D.; Sigalov, S.; Aurbach, D.; Daikhin, L. In Situ Electrochemical Quartz Crystal Admittance Methodology for Tracking Compositional and Mechanical Changes in Porous Carbon Electrodes. *J. Phys. Chem. C* **2013**, *117*, 14876–14889. [[CrossRef](#)]
18. Levi, M.D.; Sigalov, S.; Salitra, G.; Elazari, R.; Aurbach, D. Assessing the Solvation Numbers of Electrolytic Ions Confined in Carbon Nanopores under Dynamic Charging Conditions. *J. Phys. Chem. Lett.* **2011**, *2*, 120–124. [[CrossRef](#)] [[PubMed](#)]
19. Shpigel, N.; Levi, M.D.; Sigalov, S.; Daikhin, L.; Aurbach, D. In Situ Real-Time Mechanical and Morphological Characterization of Electrodes for Electrochemical Energy Storage and Conversion by Electrochemical Quartz Crystal Microbalance with Dissipation Monitoring. *Accounts Chem. Res.* **2018**, *51*, 69–79. [[CrossRef](#)]
20. Sigalov, S.; Shpigel, N.; Levi, M.D.; Feldberg, M.; Daikhin, L.; Aurbach, D. Electrochemical Quartz Crystal Microbalance with Dissipation Real-Time Hydrodynamic Spectroscopy of Porous Solids in Contact with Liquids. *Anal. Chem.* **2016**, *88*, 10151–10157. [[CrossRef](#)] [[PubMed](#)]
21. Al-Zubaidi, A.; Takahashi, M.; Ishii, Y.; Kawasaki, S. Switching of alternative electrochemical charging mechanism inside single-walled carbon nanotubes: A quartz crystal microbalance study. *RSC Adv.* **2021**, *11*, 30253–30258. [[CrossRef](#)]
22. Tsai, W.-Y.; Taberna, P.-L.; Simon, P. Electrochemical Quartz Crystal Microbalance (EQCM) Study of Ion Dynamics in Nanoporous Carbons. *J. Am. Chem. Soc.* **2014**, *136*, 8722–8728. [[CrossRef](#)]
23. Zhao, X.; Xue, P.; Hou, Y.; Jiao, Y.; Wang, Y.; Sha, Z. In situ analysis of pore size effect of ionic solvation during the formation of double electric layers. *J. Electroanal. Chem.* **2020**, *880*, 114846. [[CrossRef](#)]
24. Wu, Y.-C.; Taberna, P.-L.; Simon, P. Tracking ionic fluxes in porous carbon electrodes from aqueous electrolyte mixture at various pH. *Electrochem. Commun.* **2018**, *93*, 119–122. [[CrossRef](#)]
25. Griffin, J.M.; Forse, A.; Tsai, W.-Y.; Taberna, P.-L.; Simon, P.; Grey, C. In situ NMR and electrochemical quartz crystal microbalance techniques reveal the structure of the electrical double layer in supercapacitors. *Nat. Mater.* **2015**, *14*, 812–819. [[CrossRef](#)]
26. Shpigel, N.; Levi, M.D.; Sigalov, S.; Aurbach, D.; Daikhin, L.; Presser, V. Novel in situ multiharmonic EQCM-D approach to characterize complex carbon pore architectures for capacitive deionization of brackish water. *J. Phys. Condens. Matter.* **2016**, *28*, 114001. [[CrossRef](#)]
27. Dargel, V.; Shpigel, N.; Sigalov, S.; Nayak, P.; Levi, M.D.; Daikhin, L.; Aurbach, D. In situ real-time gravimetric and viscoelastic probing of surface films formation on lithium batteries electrodes. *Nat. Commun.* **2017**, *8*, 2081. [[CrossRef](#)]
28. Shpigel, N.; Levi, M.D.; Aurbach, D. EQCM-D technique for complex mechanical characterization of energy storage electrodes: Background and practical guide. *Energy Storage Mater.* **2019**, *21*, 399–413. [[CrossRef](#)]
29. Malka, D.; Attias, R.; Shpigel, N.; Malchick, F.; Levi, M.D.; Aurbach, D. Horizons for Modern Electrochemistry Related to Energy Storage and Conversion, a Review. *Isr. J. Chem.* **2021**, *61*, 11–25. [[CrossRef](#)]
30. Shpigel, N.; Chakraborty, A.; Malchik, F.; Bergman, G.; Nimkar, A.; Gavriel, B.; Turgeman, M.; Hong, C.N.; Lukatskaya, M.R.; Levi, M.D.; et al. Can Anions Be Inserted into MXene? *J. Am. Chem. Soc.* **2021**, *143*, 12552–12559. [[CrossRef](#)]
31. Lin, Z.; Taberna, P.-L.; Simon, P. Electrochemical double layer capacitors: What is next beyond the corner? *Curr. Opin. Electrochem.* **2017**, *6*, 115–119. [[CrossRef](#)]
32. Teran, F.E.; Arnau, A.; Garcia, J.; Jiménez, Y.; Perrot, H.; Sel, O. Gravimetric and dynamic deconvolution of global EQCM response of carbon nanotube based electrodes by Ac-electrogravimetry. *Electrochem. Commun.* **2016**, *70*, 73–77. [[CrossRef](#)]
33. Escobar-Teran, F.; Perrot, H.; Sel, O. Ion Dynamics at the Single Wall Carbon Nanotube Based Composite Electrode/Electrolyte Interface: Influence of the Cation Size and Electrolyte pH. *J. Phys. Chem. C* **2019**, *123*, 4262–4273. [[CrossRef](#)]
34. Goubaa, H.; Escobar-Teran, F.; Ressay, I.; Gao, W.; El Kadib, A.; Lucas, I.T.; Raihane, M.; Lahcini, M.; Perrot, H.; Sel, O. Dynamic Resolution of Ion Transfer in Electrochemically Reduced Graphene Oxides Revealed by Electrogravimetric Impedance. *J. Phys. Chem. C* **2017**, *121*, 9370–9380. [[CrossRef](#)]
35. Gao, W.; Debieume-Chouvy, C.; Lahcini, M.; Perrot, H.; Sel, O. Tuning Charge Storage Properties of Supercapacitive Electrodes Evidenced by In Situ Gravimetric and Viscoelastic Explorations. *Anal. Chem.* **2019**, *91*, 2885–2893. [[CrossRef](#)] [[PubMed](#)]

36. Arias, C.R.; Debiemme-Chouvy, C.; Gabrielli, C.; Laberty-Robert, C.; Pailleret, A.; Perrot, H.; Sel, O. New Insights into Pseudocapacitive Charge-Storage Mechanisms in Li-Birnessite Type MnO₂ Monitored by Fast Quartz Crystal Microbalance Methods. *J. Phys. Chem. C* **2014**, *118*, 26551–26559. [[CrossRef](#)]
37. Halim, E.M.; Elbasri, M.; Perrot, H.; Sel, O.; Lafdi, K.; El Rhazi, M. Synthesis of carbon nanofibers/poly(para-phenylenediamine)/nickel particles nanocomposite for enhanced methanol electrooxidation. *Int. J. Hydrogen Energy* **2019**, *44*, 24534–24545. [[CrossRef](#)]
38. Lemaire, P.; Sel, O.; Corte, D.A.D.; Iadecola, A.; Perrot, H.; Tarascon, J.-M. Elucidating the Origin of the Electrochemical Capacity in a Proton-Based Battery HxIrO₄ via Advanced Electrogravimetry. *ACS Appl. Mater. Interfaces* **2019**, *12*, 4510–4519. [[CrossRef](#)] [[PubMed](#)]
39. Teran, F.E.; Perrot, H.; Sel, O. Charge storage properties of single wall carbon nanotubes/Prussian blue nanocube composites studied by multi-scale coupled electrogravimetric methods. *Electrochim. Acta* **2018**, *271*, 297–304. [[CrossRef](#)]
40. Gabrielli, C.; García-Jareño, J.J.; Keddami, M.; Perrot, H.; Vicente, F. Ac-Electrogravimetry Study of Electroactive Thin Films. I. Application to Prussian Blue. *J. Phys. Chem. B* **2002**, *106*, 3182–3191. [[CrossRef](#)]
41. Gabrielli, C.; Garcia-Jareño, J.J.; Keddami, M.; Perrot, A.H.; Vicente, F. Ac-Electrogravimetry Study of Electroactive Thin Films. II. Application to Polypyrrole. *J. Phys. Chem. B* **2002**, *106*, 3192–3201. [[CrossRef](#)]
42. Levi, M.D.; Sigalov, S.; Salitra, G.; Aurbach, D.; Maier, J. The Effect of Specific Adsorption of Cations and Their Size on the Charge-Compensation Mechanism in Carbon Micropores: The Role of Anion Desorption. *ChemPhysChem* **2011**, *12*, 854–862. [[CrossRef](#)] [[PubMed](#)]
43. Bruckenstein, S.; Hillman, R. Consequences of thermodynamic restraints on solvent and ion transfer during redox switching of electroactive polymers. *J. Phys. Chem.* **1988**, *92*, 4837–4839. [[CrossRef](#)]
44. French, H.M.; Henderson, M.J.; Hillman, A.; Vieil, E. Temporal resolution of ion and solvent transfers at nickel hydroxide films exposed to LiOH. *Solid State Ionics* **2002**, *150*, 27–37. [[CrossRef](#)]
45. French, H.M.; Henderson, M.J.; Hillman, A.; Vieil, E. Ion and solvent transfer discrimination at a nickel hydroxide film exposed to LiOH by combined electrochemical quartz crystal microbalance (EQCM) and probe beam deflection (PBD) techniques. *J. Electroanal. Chem.* **2001**, *500*, 192–207. [[CrossRef](#)]
46. Gonsalves, M.; Hillman, A.R. Effect of time scale on redox-driven ion and solvent transfers at nickel hydroxide films in aqueous lithium hydroxide solutions. *J. Electroanal. Chem.* **1998**, *454*, 183–202. [[CrossRef](#)]
47. Razzaghi, F.; Debiemme-Chouvy, C.; Pillier, F.; Perrot, H.; Sel, O. Ion intercalation dynamics of electrosynthesized mesoporous WO₃ thin films studied by multi-scale coupled electrogravimetric methods. *Phys. Chem. Chem. Phys.* **2015**, *17*, 14773–14787. [[CrossRef](#)]
48. Zhao, X.; Wang, Y.; Zhu, Y.; Zhu, L.; Yang, L.; Hou, Y.; Sha, Z. Frequency-dependence of electric double layer capacitance of TiO₂-based composite nanotube arrays. *J. Electroanal. Chem.* **2016**, *779*, 199–206. [[CrossRef](#)]
49. Zhao, X.; Hou, Y.; Wang, Y.; Yang, L.; Zhu, L.; Cao, R.; Sha, Z. Prepared MnO₂ with different crystal forms as electrode materials for supercapacitors: Experimental research from hydrothermal crystallization process to electrochemical performances. *RSC Adv.* **2017**, *7*, 40286–40294. [[CrossRef](#)]
50. Alhebshi, N.A.; Salah, N.; Hussain, H.; Salah, Y.N.; Yin, J. Structural and Electrochemical Properties of Physically and Chemically Activated Carbon Nanoparticles for Supercapacitors. *Nanomaterials* **2021**, *12*, 122. [[CrossRef](#)]